Excited states of incipient Wigner molecules

S. A. Blundell* and S. Chacko†

SPSMS, UMR-E CEA/UJF-Grenoble 1, INAC, Grenoble, FR-38054, France

(Received 18 December 2010; revised manuscript received 14 March 2011; published 31 May 2011)

An accurate configuation-interaction method employing a mean-field basis set is used to study the excitation spectrum of localized Wigner states in the strongly interacting regime of a quasi-two-dimensional parabolic quantum dot with $N = 6$ electrons. The approach achieves errors of order 1 part in 10^4 (or better) in the energies of low-lying states for a Wigner-Seitz radius $r_s = 12\,a_0^*$–$16\,a_0^*$, and is used to study low-lying spin, rotational, vibrational, and isomeric excitations. The vibrational excitations at $r_s = 50\,a_0^*$ are shown to correspond qualitatively with the classical normal modes of the $N = 6$ electron dot, although the excitation energies agree only semiquantitatively with the classical normal-mode frequencies as a result of residual quantum fluctuations.

DOI: 10.1103/PhysRevB.83.195444 PACS number(s): 73.21.La, 73.22.Gk

I. INTRODUCTION

A semiconductor quantum dot (QD), or *artificial atom*, is formed when a finite number of free-carrier electrons (or holes) is confined electrostatically to a nanometer-sized region.[1] QDs are highly tunable in experiments; their size and shape, and the number and average density of the confined electrons can all be varied. This opens up the possibility of studying a finite electron system at very low electron densities, where one enters the strongly interacting regime in which the Coulomb interaction energy greatly exceeds the kinetic energy $E_{\rm Coul} \gg E_{\rm kin}$. (In contrast, real atoms or molecules have fixed sizes with $E_{\rm Coul} \approx E_{\rm kin}$.) In the strongly interacting regime, the electrons are expected to localize under their mutual Coulomb repulsion into a *Wigner molecule*,[2,3] a finite-sized analog of the electron lattice (Wigner solid) that forms in the infinite homogeneous electron gas at low density.[4] It has been possible to observe evidence of the bulk transition to a Wigner solid,[5] but the effect in finite systems has proved more elusive. Recently, however, Singha *et al.*[6] have observed low-lying excitations of a correlated two-electron molecularlike state in optically tuned GaAs quantum dots. Further advances in experimental methodology, such as improved growth techniques for semiconductor QDs, may soon make it possible to observe Wigner molecule states of several electrons in quasi-two-dimensional (2D) QDs at zero magnetic field.

Much recent theoretical work has been devoted to studying the strongly interacting regime in quantum dots.[6–12] Very precise studies of the ground and low-lying excited states of quantum dots have recently been made using a form of quantum Monte Carlo (QMC), variational Monte Carlo–diffusion Monte Carlo (VMC–DMC).[8,9,11] This approach has been applied for up to $N = 18$ electrons and down to low densities $r_s \lesssim 55\,a_0^*$. [Here, $r_s = (\pi\bar{n})^{-1/2}$ is the average Wigner-Seitz radius for a quasi-2D QD, where $\bar{n}$ is the average electron density in the plane of the dot, and a_0^* is the effective Bohr radius[1] in the semiconductor.] The VMC–DMC method is applicable to the ground state or to the lowest state of a given symmetry (such as spin S and orbital angular momentum L_z), but it can not be used to study excited states systematically.

Another approach, configuration interaction (CI),[13] is well suited to extracting excited states, but until recently its application to the strongly interacting regime has been limited to more moderate sizes N or electron densities, such as $r_s \lesssim 20\,a_0^*$ for $N = 4$ electrons in Ref. 12, or $r_s \lesssim 13\,a_0^*$ for $N = 8$ electrons in Ref. 7, with a reported precision significantly worse than that of the VMC–DMC approach discussed above. A third approach is the two-step approach,[10,14] where a Hartree-Fock solution is followed by the projection of a rotational state. The two-step method is computationally rapid but is expected to lose some accuracy in the regime of partial Wigner localization at the intermediate electron densities that concern us here.[14]

We have recently developed a high-precision CI approach for quasi-2D quantum dots that uses a numerical mean-field basis set and applied it to the high-density limit ($r_s \sim 1.7\,a_0^*$) for $3 \leqslant N \leqslant 20$ confined electrons.[15] For the smaller sizes $N \lesssim 7$, the accuracy of the energies of low-lying states was found to be comparable to or better than VMC–DMC calculations[16] for the same density. Our CI approach is particularly suited to the strongly interacting regime because the low-lying members of the mean-field basis set already "know" about the electron localization. We made an initial application of the approach to the low-density limit of the $N = 6$ electron dot in Ref. 17, where we gave evidence that the ground-state energy at $r_s \approx 12\,a_0^*$ could be extracted with an accuracy that was comparable to or better than that achieved by VMC–DMC.[9] We also used the method to study the *isomeric* excitations of the six-electron dot (that is, excitations to different geometrical arrangements of the localized electrons), finding that, at intermediate densities $r_s \lesssim 25\,a_0^*$, the isomeric excitations had lower energy than vibrational excitations for a given orbital angular momentum L_z.

This paper extends and elaborates on the work reported in Ref. 17. We give a detailed description of the CI method employed in Ref. 17, with the added refinements necessary for the strongly interacting regime, and then apply it to perform precise calculations of the energy of the lowest eight states of the six-electron dot at two densities $r_s \approx 12\,a_0^*$ and $16\,a_0^*$, comparing with other precise calculations in the literature where available. These calculations are intended to serve as benchmarks to assess the accuracy of both the present CI approach and other calculations in the literature. We also extract the spin splittings of the ground-state spin multiplet with high precision over a large range of electron densities, as well as the first rotational excitation energy, which is compared to a semiclassical estimate. We then focus on the vibrational

excited states at $r_s = 50\,a_0^*$, analyzing the excitation energies and giving a group-theoretical analysis of the allowed spins in order to make a correspondence with the classical normal modes of the six-electron dot.

Much earlier work has been devoted to studies of the vibrational and rotational excitation modes of small quantum dots with up to $N = 5$ electrons (see, for example, Refs. 18 and 19). However, parabolic quantum dots with $N \geqslant 6$ electrons in general have more than one classical isomer (that is, stable arrangements of classical point electrons in a parabolic confining potential),[20,21] and therefore isomeric states should form an important part of the phenomenology of excited states in the strongly interacting regime. For this reason, the main part of this work is a case study of the excited states of the $N = 6$ electron quasi-2D dot, which is the smallest N dot to show isomeric excited states as well as rotational, vibrational, and spin excitations. We consider a density range $2.75\,a_0^* \leqslant r_s \leqslant 50\,a_0^*$, including intermediate values of $r_s \sim 6\,a_0^*$ where the localization is only partial, but which may be accessible in initial experiments.

Note that molecularlike states can also be induced at high densities ($r_s \sim 1.5\,a_0^*$) by an intense magnetic field or by very high angular momentum,[22,23] and the molecular model of quantum dots has also been studied in this context.[10,23,24] In addition, experimental evidence for "rigid-rotor" behavior of low-angular-momentum states has recently been found[12] in a four-electron QD at high densities $r_s \sim 1.7\,a_0^*$.

The plan of this paper is as follows. In the next section, we describe our CI method as applied to the strongly interacting regime and carry out test calculations to demonstrate its convergence properties. In Sec. III, we then use the method to calculate precise energies of low-lying states to compare to other precise calculations in the literature. Section IV is devoted mainly to vibrational excitations. To motivate this discussion, we begin in Sec. IV A with a discussion of the classical limit ($r_s \to \infty$); Sec. IV B then analyzes the vibrational excitations at low density and compares with the normal modes of the classical model. Although the main part of the work is for the $N = 6$ electron dot, we give arguments in Sec. IV D as to why many of our conclusions should be expected to generalize to higher N. The conclusions are summarized in Sec. V.

II. METHOD

We consider the confined electron gas to be quasi-2D and wish to solve for the many-body envelope wave function in the effective mass approximation.[25] The N-electron Hamiltonian is taken to be

$$H = \sum_{i=1}^{N}\left[-\frac{\nabla_i^2}{2m^*} + V_{\rm ext}(r_i)\right] + \sum_{i<j}^{N}\frac{e^2}{(4\pi\epsilon_0)\epsilon|\mathbf{r}_i - \mathbf{r}_j|}\,, \quad (1)$$

where m^* is the effective mass in the conduction band of the semiconductor, ϵ is the dielectric constant, $V_{\rm ext}(r)$ is the external confining potential, and the vectors $\mathbf{r}$ are 2D. We consider here confinement by a circular parabolic potential

$$V_{\rm ext}(r) = \tfrac{1}{2}m^*\omega^2 r^2\,. \quad (2)$$

Throughout this paper, we work in *effective* atomic units (a.u.) corresponding to scaled coordinates with lengths expressed in units of $a_0^* = (\epsilon/m^*)a_0$, where a_0 is the Bohr radius, and energies in units of $\mathrm{Ha}^* = (m^*/\epsilon^2)$ Ha. One can thus effectively set $m^* = \epsilon = e = (4\pi\epsilon_0) = 1$ in Eq. (1) and, accordingly, we drop m^* and ϵ and the other constants from most of the subsequent equations.

The average density $\bar{n}$ of the confined electrons is controlled by the harmonic frequency ω in Eq. (2). We use as our density parameter the average Wigner-Seitz radius $r_s = (\pi\bar{n})^{-1/2}$, which is given approximately by[26]

$$r_s^3 = \frac{1}{\omega^2\sqrt{N}} \quad (3)$$

(in effective a.u.). We take this equation to *define* r_s in terms of ω. An alternative density parameter is $\lambda = l_0/a_0^*$, the ratio of the confinement length scale $l_0 = \sqrt{\hbar/m^*\omega}$ to the effective Bohr radius; it is related to the Wigner-Seitz radius r_s defined in Eq. (3) by $r_s^3 = \lambda^4/\sqrt{N}$ (in effective a.u.).

We solve the Schrödinger equation $H\Psi = E\Psi$ by a CI approach,[13] in which the many-electron envelope function Ψ is expanded in terms of Slater determinants (configurations) Φ_α,

$$\Psi = \sum_\alpha c_\alpha \Phi_\alpha\,. \quad (4)$$

In our recently developed CI approach,[15] the Slater determinants are built from a single-particle basis of mean-field type generated numerically on a 2D Cartesian grid. However, even when as here the external potential $V_{\rm ext}(r)$ is circularly symmetric, in the low-density limit, mean-field approaches such as Hartree-Fock (HF) or mean-field-like methods such as spin-density functional theory generally yield an electronic density with broken circular symmetry displaying localized electrons.[3] It is inconvenient here to use such a mean-field potential to generate the single-particle basis because the single-particle states would not then have definite orbital angular momentum ℓ_z. Consequently, it would not be possible to reduce the number of configurations included in Eq. (4) by restricting the Slater determinants Φ_α to those with a definite total orbital angular momentum L_z, which is an exact quantum number for a circularly symmetric external potential. Moreover, a basic theorem[27] for the 2D electron gas states that, when the external confining potential is circularly symmetric, the exact one-body density (in the laboratory frame) is also circularly symmetric for a state of definite total orbital angular momentum L_z. If we used a basis set for a broken-symmetry mean field, these symmetries of the exact solution would only be recovered in the limit of full CI (that is, all possible Slater determinants included) and single-particle basis-set completeness (no upper energy cutoff to the basis).[15]

Instead, to generate the single-particle basis set, we choose an approximate mean-field potential that is circularly symmetrized. First, we construct an approximate analytical one-body density as a sum of M concentric Gaussian rings

$$\rho_0(r) = \sum_{I=1}^{M} N_I \exp[-\alpha_I(r - R_I)^2]\,. \quad (5)$$

TABLE I. CI energies of the ground state ($S = 0$) and the lowest-lying $S = 3$ state of an $N = 6$ electron dot for density parameter $\lambda = 8$ ($r_s \approx 12\,a_0^*$) using a model space formed from either 10 [$v10$] or 8 [$v8$] single-particle orbitals. The notation [$v8'$] indicates a model space of size 8 with a modified single-particle potential (see text). QMC: variational-diffusion quantum Monte Carlo, with the quoted error being statistical. Units: Ha*.

Excitation	$S = 0$ [$v10$]	$S = 0$ [$v8$]	$S = 0$ [$v8'$]	$S = 3$ [$v10$]	$S = 3$ [$v8$]
Lowest order	0.96757	0.97614	0.99313	0.96170	0.96841
Singles	−0.01695(2)	−0.01991(2)	−0.03007(3)	−0.01127(2)	−0.01372(2)
Doubles	−0.00672(2)	−0.01024(2)	−0.01552(2)	−0.00559(3)	−0.00842(3)
Triples	−0.00154(4)	−0.00312(4)	−0.00457(5)	−0.00111	−0.00215
Quadruples	−0.00026(3)	−0.00072(3)	−0.00085(2)	−0.00017(2)	−0.00052(3)
Pentuples	−0.00002	−0.00008(1)	−0.00009(1)	−0.00001	−0.00005(1)
Hextuples	0.00000	−0.00001	0.00000(1)	0.00000	0.00000
Total	0.94206(6)	0.94208(6)	0.94204(7)	0.94354(4)	0.94355(5)
QMC, Ref. 9	0.942580(5)			0.943631(3)	

The ring radii R_I and width parameters α_I are chosen either by minimizing a semiclassical (extended Thomas-Fermi) energy functional[28] or by performing an unrestricted HF calculation. These approaches generally give broken-symmetry solutions[3] with localized electrons in a pattern of concentric rings, thus permitting suitable values for R_I and α_I to be estimated; we choose the R_I as the radius of each ring, and α_I can be based on the width of a single localized electron peak. The normalization parameters N_I can then be chosen to fix the number of electrons in each ring.

Finally, we generate the single-particle basis in the Kohn-Sham effective potential[28] $V_{\rm eff}[\rho_0](r)$ corresponding to the density ρ_0, following the procedure described in Ref. 15. The potential $V_{\rm eff}[\rho_0](r)$ is also circularly symmetric, and the single-particle states can therefore have definite ℓ_z with the form

$$\psi_j(\mathbf{r}) = \exp(im_j\theta) f_j(r)\,, \tag{6}$$

where $f_j(r)$ is a radial function and m_j an angular quantum number. The low-lying members of the basis typically have charge density $|\psi_j(\mathbf{r})|^2 = |f_j(r)|^2$ located in the vicinity of the ring radii R_I, and in this sense the set forms an efficient basis for constructing a CI solution. As we shall see, there does not seem to be much difference in the performance of the basis for small variations in the parameters R_I or α_I. In principle, one could optimize R_I and α_I by taking improved estimates iteratively from the CI solution, but at least in the examples presented here, one gains little from this procedure. Since the basis states have definite ℓ_z, it is now easy to arrange for the CI solution to have definite L_z (and spin), and for the density to be circularly symmetric, for any truncation of the configurations included, which is very convenient.

III. ENERGY OF LOW-LYING STATES

In this section, we use our CI method to calculate the energy of the ground and low-lying excited states of the $N = 6$ electron dot in order to compare with other precise calculations in the literature, at the same time describing further aspects of our methodology. We consider two intermediate densities $\lambda = 8$ ($r_s \approx 12\,a_0^*$) and $\lambda = 10$ ($r_s \approx 16\,a_0^*$), where the low-lying states are spin and rotational excitations of the ground state.

Table I shows full CI calculations for the ^1S ground state and lowest ^7S excited state. Following the general procedure of Ref. 15, we employ a *model space* consisting of all determinants that can be formed by distributing the electrons over the lowest 8 or 10 orbitals in the basis, and we then consider successively all possible single, double, ..., etc., excitations from this model space up to the full CI limit (hextuple excitations). For any given truncation (to triples, say), we perform the calculation for a series of upper energy cutoffs $\epsilon_{\rm cut}$ to the single-particle basis, and we then extrapolate this cutoff to infinity $\epsilon_{\rm cut} \to \infty$ as described in Ref. 15. The only significant error in this entire procedure is the error in these extrapolations; we perform the extrapolation separately for each degree of excitation and show an estimate of the error in the table. Although the contributions from each degree of excitation differ, the two different sizes of model space give the same final total energy to within the estimated extrapolation errors. This is an important consistency check in our calculation.

In Table I, we have also considered basis sets for two different potentials for the ^1S ground state. The first (used for the columns $v8$ and $v10$) uses ring radii R_I and widths α_I [Eq. (5)] estimated by minimizing a semiclassical energy functional. This minimization yields a Wigner molecule with a central electron and an outer ring of five electrons in a pentagonal arrangement (see Sec. IV); for a density parameter $\lambda = 8$, we obtain $(R_1,\alpha_1) = (0,6.3)$ and $(R_2,\alpha_2) = (22.4,7.0)$ (in effective a.u.). The converged CI calculation gives a radius for the outer ring of $R_{2,\rm CI} = 21.6\,a_0^*$, so the parameters obtained from the semiclassical minimization are quite physical. For the second potential (used for the column $v8'$), we have modified these parameters somewhat to $(R_1',\alpha_1') = (0,8.3)$ and $(R_2',\alpha_2') = (20.0,9.0)$. Once again, we find agreement in the final totals to within our estimated extrapolation error. Note that the $v8'$ calculation displays a somewhat slower rate of convergence than the $v8$ calculation, reflecting the fact that the second potential is less physical. However, the overall extrapolation error is comparable to that obtained from the first potential.

We have used this procedure to calculate the energies of the ground state and the first eight excited states at two densities, $\lambda = 8$ and $\lambda = 10$ (see Table II). All the energies in this

TABLE II. Energy of the ground state and the first eight excited states of the $N = 6$ electron dot for two densities: $\lambda = 8$ ($r_s \approx 12\,a_0^*$) and $\lambda = 10$ ($r_s \approx 16\,a_0^*$). CI: configuration interaction; VMC–DMC: variational-diffusion quantum Monte Carlo, with the quoted error being statistical. PIMC: path-integral quantum Monte Carlo. Units: Ha*.

λ	S	L_z	CI (This paper)	VMC–DMC (Ref. 9)	CI (Ref. 7)	PIMC (Ref. 2)
8	0	0	0.94206(6)	0.942580(5)	0.9475	
	2	0	0.94279(5)	0.943000(3)	0.9489	
	1	1	0.94280(5)	0.943792(5)	0.9486	0.9433(3)
	1	0	0.94350(4)			
	3	0	0.94355(4)	0.943631(3)	0.9500	0.9441(3)
	2	1	0.94360(3)			
	1	1	0.94365(4)			
	0	1	0.94378(5)			
	0	2	0.94378(4)			
10	0	0	0.68896(11)	0.689202(5)	0.6974	
	2	0	0.68916(9)	0.689254(6)	0.6981	
	1	1	0.68924(10)	0.690568(7)		
	1	0	0.68938(9)			
	3	0	0.68938(9)	0.689458(4)	0.6986	
	2	1	0.68947(9)			
	1	1	0.68951(10)			
	0	1	0.68954(10)			
	0	2	0.68968(10)			

table have been checked by calculating them at least twice, either with different sizes of model space, or with different basis-set potentials. Note that our energies are systematically lower (more negative) than those of Ghosal *et al.*,[9] who used a VMC–DMC method. For instance, our ^1S ground-state energy is about 0.5 mHa* less than the VMC–DMC value, a discrepancy which is about 100 times the statistical error in the VMC–DMC value and about 10 times our estimated error. Now, the VMC–DMC energy may be regarded as a variational upper bound to the true energy, containing a systematic error due to the fixed-node approximation used in DMC step; this fixed-node error is difficult to estimate within the approach, but is expected to be small.[9] Since all our values are lower (more negative) than the VMC–DMC values, a possible explanation for the discrepancies is that we have revealed the fixed-node error in the VMC–DMC. A similar conclusion was reached[15] at high densities ($r_s \approx 1.7\,a_0^*$) in a comparison between our CI approach and another VMC–DMC calculation.[16] Our CI energies are also lower than those from a different CI approach,[7] which employs a simple-harmonic-oscillator (SHO) basis set; the SHO basis set is less efficient for describing the low-density regime than the basis set employed here. However, we note that the energy orderings of the ^3P and ^7S states in the two CI approaches agree (with ^3P having lower energy), but disagree with the ordering given by VMC–DMC. Finally, we note that there are two ^1P states among the first eight excited states, which can both be calculated by CI; in contrast, only the lowest-energy state of a given symmetry can be studied by VMC–DMC, which is essentially a variational method.

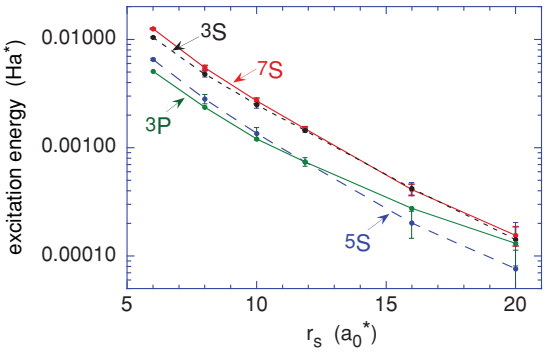

FIG. 1. (Color online) Excitation energy relative to the ^1S ground state of the lowest-lying ^3S, ^5S, ^7S, and ^3P states of the $N = 6$ electron dot versus Wigner-Seitz radius r_s [Eq. (3)].

In Fig. 1, we show the evolution of the excitation energy of the lowest ^3S, ^5S, ^7S, and ^3P states relative to the ^1S ground state for $6\,a_0^* \leqslant r_s \leqslant 20\,a_0^*$. The three S-wave states (members of the S-wave ground-state spin multiplet) yield approximately parallel straight lines on a logarithmic plot, the excitation energy ΔE of these states being well fit in this range of r_s by an expression of the form $\Delta E = c\exp(-mr_s)$, with $c(^3S) = 0.048$ Ha*, $c(^5S) = 0.028$ Ha*, and $c(^7S) = 0.054$ Ha*. The constant $m \approx 0.30\,(a_0^*)^{-1}$ for all three states. Therefore, if one considered a Heisenberg-type model for the spin-spin interactions of localized electrons $H_{\rm spin} = \sum_{\{ij\}} J_{ij}\mathbf{S}_i \cdot \mathbf{S}_j$, this result would imply that the effective spin couplings J_{ij} decrease approximately exponentially with r_s, $J_{ij} \sim \exp(-mr_s)$, with $m \approx 0.30\,(a_0^*)^{-1}$ in the range $6\,a_0^* \leqslant r_s \leqslant 20\,a_0^*$. The ^3P state, however, shows a clear curvature on the logarithmic plot, which arises from a rotational contribution to the excitation energy with an approximate r_s^{-2} dependence (from the moment of inertia, see Sec. IV A). This contribution will eventually become dominant at large $r_s \gtrsim 15\,a_0^*$ as the spin splittings become smaller than the rotational energies (see Sec. IV A for a further discussion).

IV. LOW-LYING EXCITATIONS

A. Classical limit

At very low densities ($r_s \to \infty$), the localized electronic system may be described as a classical vibrating and rotating Wigner (or electron) molecule.[18,19,23] There is also the possibility of excitations to different geometrical arrangements of the localized electrons, or *isomers*.[17] The stable configurations of classical pointlike electrons in a parabolic confining potential have been considered by Bolton and Rössler[20] and by Bedanov and Peeters.[21] These authors used a simulated annealing strategy to find the minima (stable configurations) of the classical energy

$$E_{\rm cl}(\{\mathbf{r}_i\}) = \sum_i^N \frac{1}{2}\omega^2 r_i^2 + \sum_{i>j}^N \frac{1}{r_{ij}} \qquad (7)$$

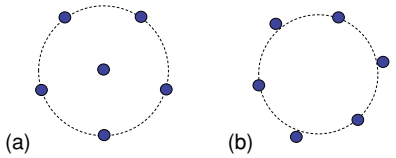

FIG. 2. (Color online) Stable configurations of the classical six-electron parabolic dot (from Ref. 20): (a) pentagonal ground-state configuration and (b) excited isomer (staggered hexagon).

(in effective a.u.). If we further rescale coordinates as $\mathbf{r}_i \to \omega^{-2/3}\mathbf{s}_i$, this becomes equivalent to minimizing

$$E_{\rm cl}(\{\mathbf{s}_i\}) \equiv \omega^{-2/3} E_{\rm cl}(\{\mathbf{r}_i\}) = \sum_i^N \frac{1}{2} s_i^2 + \sum_{i>j}^N \frac{1}{s_{ij}}, \qquad (8)$$

showing that the energy of a stable classical configuration scales as $E_{\rm cl} \propto \omega^{2/3}$ and that distances (such as bond lengths d_{ij}) scale as $d_{ij} \propto \omega^{-2/3}$.

We have repeated the search for the global minimum-energy configuration and excited isomers using a basin-hopping[29] algorithm. The stable configurations for the six-electron dot are shown in Fig. 2; in agreement with Ref. 20, the ground-state configuration is a pentagonal (1,5) arrangement and there is an excited (0,6) isomer in the form of a staggered hexagon. (We find that the perfect hexagon is a saddle point on the potential-energy surface.) These configurations have energy

$$E_{\rm cl}(1,5) = 13.355\,87\,\omega^{2/3}, \quad E_{\rm cl}(0,6) = 13.452\,08\,\omega^{2/3}, \quad (9)$$

that of the ground state agreeing with the value found in Ref. 21. By using Eq. (3) to define r_s in terms of ω, we then obtain for the isomeric excitation energy (in effective a.u.)[17]

$$\Delta E_{\rm iso} \equiv E_{\rm cl}(0,6) - E_{\rm cl}(1,5) = 0.0714\, r_s^{-1}. \qquad (10)$$

Now, at large r_s, the quantum excitation energy of a quasi-2D Wigner molecule may be written approximately in a way analogous to that for a planar molecule[30]

$$E(K) = E_{\rm cl}(K) + \frac{L_z^2}{2I_K} + \sum_\alpha \Omega_\alpha^{(K)}(n_\alpha + 1/2) + E_{\rm spin}, \quad (11)$$

where $E_{\rm cl}(K)$ is the classical energy of isomer K [Eq. (9)], I_K is its moment of inertia, and n_α is the number of vibrational quanta in a normal mode with frequency $\Omega_\alpha^{(K)}$. The energy $E_{\rm spin}$ is the spin-spin interaction energy of the spins of the localized electrons. As an example of a typical rotational excitation energy, we note that the ground-state (1,5) isomer has a moment of inertia $I_K = 8.904\,\omega^{-4/3}$, and it then follows using Eqs. (3) and (11) that the S- to P-wave excitation energy is given in the classical limit by (in effective a.u.)[17]

$$\Delta E_{\rm rot} = 0.0309\, r_s^{-2}. \qquad (12)$$

Similarly, noting that the frequency of the first classical normal mode of the (1,5) isomer is $\Omega_1 = 0.650\,\omega$ (see Sec. IV B), we find that the excitation energy of one vibrational quantum in this mode is (in effective a.u.)[17]

$$\Delta E_{\rm vib} = 0.415\, r_s^{-3/2}. \qquad (13)$$

Owing to the differing dependence on the length scale r_s displayed in Eqs. (10), (12), and (13), for sufficiently large $r_s \to \infty$, the rotational, vibrational, and isomeric excitation energies must eventually satisfy

$$\Delta E_{\rm iso} \gg \Delta E_{\rm vib} \gg \Delta E_{\rm rot}, \qquad (14)$$

analogously to the Born-Oppenheimer (BO) approximation in molecular physics.[30] However, this separation of energy scales is not necessarily satisfied at the intermediate values of r_s that may be accessible in initial experiments. Indeed, as we showed in Ref. 17, there is a crossover between $\Delta E_{\rm iso}$ and $\Delta E_{\rm vib}$, which is expected to occur around $r_s \approx 34\,a_0^*$ using the classical estimates of excitations energies (10) and (13), and which was found to occur between $r_s = 25\,a_0^*$ and $30\,a_0^*$ from CI calculations. At smaller $r_s \lesssim 25\,a_0^*$, there is an inversion of the BO-type energy ordering of Eq. (14), with the isomeric excitation energy comparable to or smaller than the vibrational excitation energy.

To clarify the role of rotational excitations, we show in Fig. 3 the classical estimate of the S- to P-wave excitation energy $\Delta E_{\rm rot}$ as a function of r_s, together with the excitation energy calculated by CI (from the ground ^1S state to the lowest ^3P state, which is the lowest-lying P-wave state). We also show a typical spin excitation energy $\Delta E(^3S)$, defined as the energy of the lowest ^3S state relative to the ^1S ground state, as calculated by CI. From Fig. 3, one sees that the smallest rotational excitation for $r_s \lesssim 10\,a_0^*$ is, in fact, somewhat larger than the classical estimate $\Delta E_{\rm rot}$. This is simply because a spin excitation is also involved. Moreover, the ^1P states are even higher in energy than the ^3P state (see Table II). The allowed spin couplings are constrained by the Pauli exclusion principle and the symmetry of the wave function, including orbital angular momentum L_z (see the Appendix), so there can again be an indirect effect of atomiclike exchange and correlation effects, responsible for spin excitations, even for ^1P states. However, as Fig. 1 shows, the spin couplings decrease

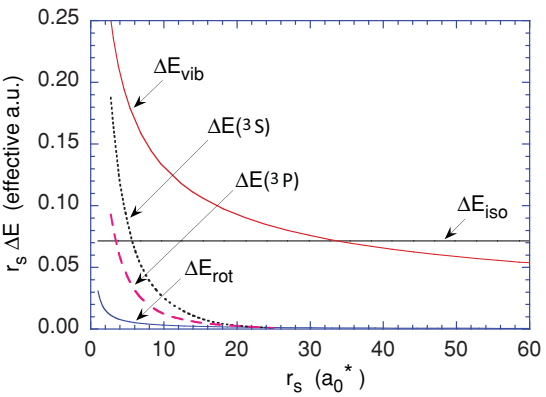

FIG. 3. (Color online) Excitation energies of the six-electron dot versus Wigner-Seitz radius r_s (partly taken from Ref. 17). The quantities $\Delta E_{\rm rot}$, $\Delta E_{\rm vib}$, and $\Delta E_{\rm iso}$ are approximate rotational, vibrational, and isomeric excitation energies, respectively, inferred from a classical model (see text); $\Delta E(^3S)$ and $\Delta E(^3P)$ are excitation energies to the lowest ^3S and ^3P states calculated by CI. All excitation energies are scaled by r_s.

approximately exponentially with r_s, so that, for sufficiently large r_s, we will eventually find

$$\Delta E_{\rm rot} \gg \Delta E_{\rm spin}\,. \tag{15}$$

The crossover is seen in Fig. 1 to occur for $r_s \approx 15\,a_0^*$, and as r_s increases further, the rotational energy starts to dominate the spin energy. The classical estimate $\Delta E_{\rm rot}$ then becomes accurate for $r_s \gg 15\,a_0^*$.

One also sees in Fig. 3 that, for $r_s \lesssim 6\,a_0^*$, the "spin" excitation energy (due to atomiclike exchange and correlation effects) is nominally comparable to the isomeric and vibrational energies. Thus, although at these values of r_s it is possible to find partial Wigner localization in a recognizable geometry (see Sec. IV C and, for example, Refs. 8 and 31), it is not generally possible to discuss isomeric and vibrational excitations separately from spin excitations at these densities.

B. Vibrational normal modes

As mentioned above, in Ref. 17 we found evidence for a crossover around $r_s = 25\,a_0^*$–$30\,a_0^*$ between the (0,6) excited isomer and the first vibrational excitation of the (1,5) ground-state isomer. We showed there that, for $r_s > 30\,a_0^*$, the excited states involved both (1,5) and (0,6) geometries, and interpreted the (1,5) geometries as vibrational excitations of the ground state. In this section, we explore further the interpretation of the excited (1,5) isomers as vibrational excitations.

Low-lying excited states at $r_s = 50\,a_0^*$ are shown in Fig. 4. In order to focus on vibrational and isomeric excitations rather than rotational excitations, we here restrict to S-wave states ($L_z = 0$). At $r_s = 50\,a_0^*$, the typical vibrational and isomeric excitation energies are of order several mHa* (see Fig. 3),

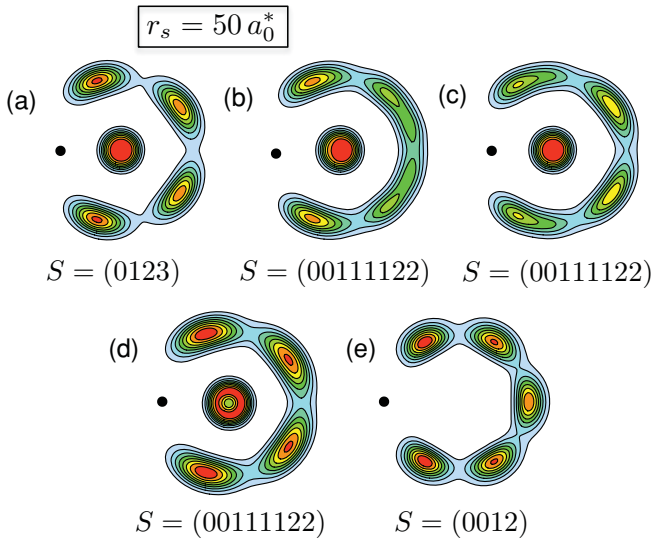

FIG. 4. (Color online) Charge-charge pair-correlation functions $g(\mathbf{r},\mathbf{r}_0)$ of low-lying S-wave states for $N = 6$ electrons for $r_s = 50\,a_0^*$ (partly taken from Ref. 17). We show representative PCFs for each spin multiplet. (a) Ground-state spin multiplet; (b)–(e) first to fourth excited S-wave spin multiplets, respectively. The position $\mathbf{r}_0$ of the reference electron is indicated by a dot, and the set of total spins S present in each multiplet is shown.

while the spin excitation energies are very small, $\Delta E_{\rm spin} \ll 0.05$ mHa*. Therefore, the excitation spectrum for fixed L_z consists of a series of nearly degenerate "spin multiplets," with a fine structure due to the spin-spin interaction and separated by a few mHa* due to vibrational and isomeric excitations. Now, as mentioned earlier, for a circularly symmetric external potential and a state of definite L_z, the electronic density (in the laboratory frame) in 2D must also be circularly symmetric,[27] and in the Wigner limit the density therefore becomes a series of concentric rings (see, for example, Ref. 8). To reveal the Wigner localization, we therefore consider the internal many-body correlations by means of the electronic (charge-charge) pair-correlation functions (PCFs) $g(\mathbf{r},\mathbf{r}_0)$,[19,23,31]

$$g(\mathbf{r},\mathbf{r}_0) = \langle\Psi|\sum_{i\neq j}\delta(\mathbf{r}_i-\mathbf{r})\delta(\mathbf{r}_j-\mathbf{r}_0)|\Psi\rangle\,, \tag{16}$$

where $\mathbf{r}_i$ is the position of electron i, and the many-body wave function $|\Psi\rangle$ is given in the CI representation by Eq. (4). The quantity $g(\mathbf{r},\mathbf{r}_0)$ is proportional to the conditional probability of finding an electron at the position $\mathbf{r}$ given that another electron is present at $\mathbf{r}_0$. For high $r_s \sim 50\,a_0^*$, the PCFs for each state in a spin multiplet are nearly the same, and so we show only a representative PCF for each multiplet in Fig. 4. One sees that the first three excited multiplets have underlying (1,5) geometry, while the fourth is a (0,6) isomeric excitation.

The classical normal modes for the ground-state isomer of the classical model [Eq. (7)] are shown in Fig. 5. There

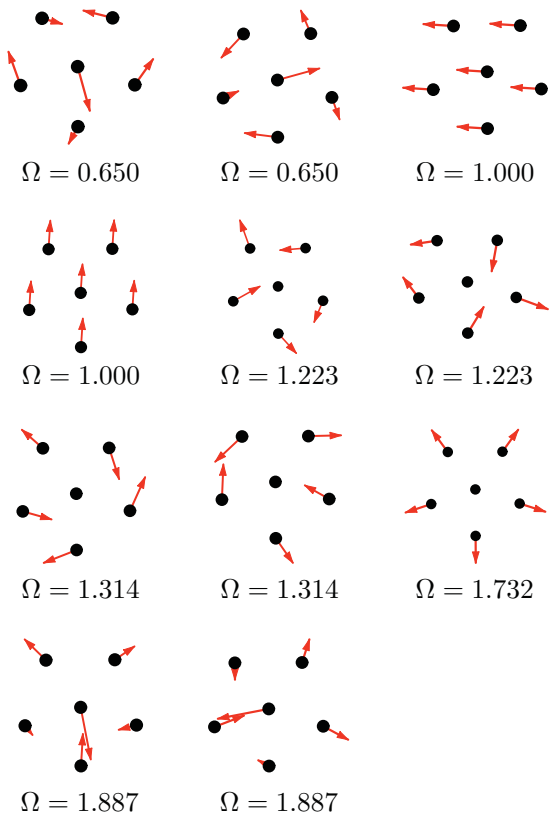

FIG. 5. (Color online) Normal modes of the ground-state isomer of the classical six-electron dot. The normal-mode frequency Ω is indicated as a multiple of the frequency ω of the parabolic confinement potential [Eq. (2)].

TABLE III. Excitation energies δE of vibrational spin multiplets relative to the ground-state multiplet for the $N = 6$ electron dot at $r_s = 50\,a_0^*$. The notations (b), (c), and (d) refer to the spin multiplets shown in Fig. 4, while [$v11$] and [$v13$] indicate use of a model space of size 11 and 13, respectively. Units: mHa*.

Excitation	δE(b) [$v11$]	δE(b) [$v13$]	δE(c) [$v11$]	δE(c) [$v13$]	δE(d) [$v11$]	δE(d) [$v13$]
Lowest order	4.25	3.77	6.91	5.64	8.77	7.73
Singles	−2.01(3)	−1.87(2)	−4.39(10)	−3.43(10)	−5.22(8)	−4.82(8)
Doubles	−0.69(5)	−0.47(4)	−0.59(5)	−0.60(9)	−1.08(2)	−0.63(9)
Triples	−0.29(3)	−0.17(2)	−0.47(8)	−0.26(1)	−0.35(27)	−0.36(10)
Quadruples	−0.02(1)	−0.01	−0.09(2)	−0.01	−0.19(5)	−0.06(2)
Pentuples	0.00	0.00	−0.02(1)	0.00	−0.01	0.00
Hextuples	0.00	0.00	0.00	0.00	0.00	0.00
Total	1.25(10)	1.26(7)	1.35(17)	1.33(16)	1.92(35)	1.87(19)

are $2N - 1 = 11$ normal modes grouped into five doubly degenerate modes and one nondegenerate mode, which is a breathing mode at high frequency. The lowest-frequency mode can be thought of as a dipolar oscillation of the central electron accompanied by a distortion of the outer ring. The third and fourth modes, at $\Omega = 1.223\,\omega$ and $1.314\,\omega$, correspond to quadrupole and octupole distortions, respectively, of the outer ring, with the central electron remaining fixed. The second mode is a collective dipolar oscillation of the center of mass (c.m.) of the system at frequency $\Omega = \omega$ (exactly), in which the whole structure remains undistorted during the oscillation. The existence of such a classical mode can be shown to be a general result for a system in a harmonic confining potential having an interaction depending only on the relative coordinates of the particles. The quantum-mechanical analog of this result is the Kohn theorem,[1] according to which under the same circumstances the c.m. motion decouples exactly from the "relative coordinates," and one can describe the system by a wave function in relative coordinates combined with oscillations of the c.m. in the harmonic confining potential.

Thus, if the ground-state energy is E_0, there will exist an excited state (Kohn mode) with one vibrational quantum in the c.m. mode having energy $E_0 + \omega$. One quantum in a simple-harmonic oscillator yields a P-wave state, and, since in the present case the ground state is a ^1S state, it follows that the Kohn mode must be a P wave overall. However, according to Eq. (12), the rotational excitation energy at $r_s = 50\,a_0^*$ is $\Delta E_{\rm rot} \approx 0.01$ mHa*, which is small compared to the excitation energy of the Kohn mode $\Delta E_K = \omega \approx 1.81$ mHa*. Thus, it should be possible to find an S-wave state with an excitation energy close to $\Delta E \approx 1.81$ mHa* corresponding to the collective normal mode.

In Table III, we make an extrapolation of the excitation energy of the three excited (1,5) multiplets in Fig. 4 to the limit of basis-set completeness. For the purposes of the calculation, we here define the excitation energy as the difference between the energy of spin $S = 2$ states of the ground state and excited multiplets (although this choice of S is immaterial since the spin energy at $r_s = 50\,a_0^*$ is tiny, and is also much smaller than our numerical error). The convergence of the excitation energies with respect to the upper cutoff of the basis set is rather slow at this large value of r_s, and the extrapolation errors have accordingly been estimated as rather large, but as a check we have obtained agreement with calculations performed with two different sizes of model space. According to these results, of the three multiplets, Figs. 4(b), 4(c), and 4(d), only (d) is energetically consistent with the collective Kohn-type oscillation.

Further insight into the nature of the (1,5) excited multiplets may be gained by considering the sets of total spins present in the multiplet as a function of the total orbital angular momentum L_z, which are shown in Table IV. The spins in this table were obtained directly from the CI diagonalization, but they can also be shown to emerge from symmetry considerations (see the Appendix). Thus, the set of spins for the ground state $S = (0123)$ for $L_z = 0$ and $S = (0112)$ for $1 \leqslant L_z \leqslant 4$ is just that required for the C_{5v} pentagonal internal symmetry of the state; this pattern repeats with a periodicity of 5 (so that $L_z = 5$ is equivalent to $L_z = 0$) related to the five-fold symmetry of the state. Similarly, for the (0,6) isomer [column (e) in Table IV], the set of allowed spins corresponds to a C_{6v} hexagonal internal symmetry and repeats with a periodicity of 6. It is interesting that the corresponding classical isomer [see Fig. 2(b)] has a slight distortion from exact C_{6v} symmetry since there are two groups of three electrons with slightly different radii, resulting in only three-fold symmetry. One can show that the allowed spins for this lower symmetry for $L_z = 0$ would be $S = (00011123)$, which is not what is found in our calculations. As emphasized by Bolton and Rössler,[20] the classical potential-energy surface for this isomer

TABLE IV. Total spin quantum numbers present in low-lying spin multiplets of the $N = 6$ electron dot at $r_s = 50\,a_0^*$ as a function of total orbital angular momentum L_z. The notations (a)–(e) refer to the spin multiplets shown in Fig. 4: (a) is the ground-state multiplet, and (b)–(e) are the first to fourth excited multiplets, respectively. Notation: An entry such as (0112) indicates that four levels are present in the multiplet, with total spins $S = 0$, 1 (twice), and 2.

L_z	(a)	(b)	(c)	(d)	(e)
0	(0123)	(00111122)	(00111122)	(00111122)	(0012)
1	(0112)	(00111223)	(00111122)	(00111223)	(112)
2	(0112)	(00111122)	(00111223)	(00111122)	(012)
3	(0112)	(00111122)	(00111223)	(00111122)	(0113)
4	(0112)	(00111223)	(00111122)	(00111223)	(012)
5	(0123)	(00111122)	(00111122)	(00111122)	(112)
6	(0112)	(00111223)	(00111122)	(00111223)	(0012)

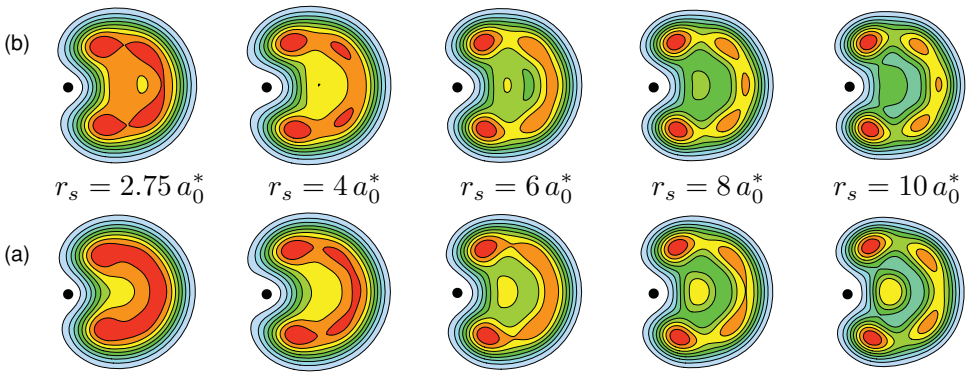

FIG. 6. (Color online) Charge-charge pair-correlation functions $g(\mathbf{r},\mathbf{r}_0)$ of (a) the ^1S ground state, and (b) the first excited ^1S state of the $N = 6$ electron dot at high-to-intermediate electron densities. The position $\mathbf{r}_0$ of the reference electron is indicated by a dot.

in the vicinity of the perfect and staggered hexagons is very flat. It is possible that, when the localized electrons are of finite width (as they are for $r_s = 50\,a_0^*$) rather than pointlike (as in the classical model), the exact C_{6v} symmetry is preferred.

Turning to the excited (1,5) isomers [columns (b), (c), and (d) in Table IV], we note that (b) and (d) have the same pattern of spins, but (c) has a different pattern. In the Appendix, we show that (b), (c), and (d) are consistent with one vibrational quantum in three different normal modes. The larger number of allowed spin values compared to the ground (1,5) isomer (eight spin values instead of four) is related to the two-fold degeneracy of the normal modes. Further, as we show in the Appendix, the pattern of spins for (b) and (d) corresponds to a normal mode with dipolar symmetry, while that for (c) corresponds to a normal mode with either quadrupolar or octupolar symmetry. Now, the first two classical normal modes in Fig. 5 have dipolar symmetry, and the third is quadrupolar (see the Appendix). It is natural to assume that the excitation energy of a quadrupolar mode is lower than that of an octupolar mode (as is the case for the classical normal modes, Fig. 5). Thus, the spin signatures and the excitation-energy analysis suggest a tentative correspondence of (b) with the first classical normal mode (at $\Omega = 0.650\,\omega$), (c) with the third (at $\Omega = 1.223\,\omega$), and (d) with the collective mode (at $\Omega = \omega$). Note that the excitation energies found in Table IV are of the right order of magnitude for this correspondence, but do not agree precisely with the classical values. In particular, the correspondence involves an inversion of the energy ordering of the second and third classical modes relative to the quantum result. Once again, this can be attributed to the finite localization width (and residual quantum fluctuations) at $r_s = 50\,a_0^*$.

C. Isomeric hybridization for $r_s \lesssim 10\,a_0^*$

In Ref. 17, it was observed that the (1,5) and (0,6) isomers could quantum mechanically hybridize when a vibrational and an isomeric excitation occurred at nearby energies, as in the vicinity of the vibrational-isomeric crossovers, which were shown to occur for $r_s \gtrsim 25\,a_0^*$. Thus, the PCF for the (0,6) structure acquired a small central peak, and that for the (1,5) structure showed evidence of a weak sixth peak in the outer ring. At higher densities $r_s \lesssim 10\,a_0^*$, one also finds isomeric hybridization, but of a different type, this time involving hybridization between the ^1S ground state and the first excited ^1S state.

Charge-charge PCFs for these two ^1S states are shown in Fig. 6 for various values of r_s. The images here have been rescaled to have the same size for each r_s; the radius of the outer ring is in fact given approximately by $R_{\rm ring} \approx 1.7\,r_s$. Now, the "equilibrium" density (that is, the density at which the total energy of the system is minimized) for a quasi-2D quantum dot is around $r_s \approx 1.4\,a_0^*$–$1.8\,a_0^*$, a density that occurs in many experiments.[1] At equilibrium densities, the electronic structure is described approximately by an atomiclike shell model,[1] and as we have seen, as the density is reduced from its equilibrium value, one eventually finds Wigner localization. The onset of Wigner localization in a quantum dot with a small, finite number of electrons is not a sharp transition but evolves gradually as a function of r_s (see, for example, Ref. 8). As can be seen from Fig. 6, even at slightly lower densities $r_s \approx 2.75\,a_0^*$–$4\,a_0^*$ than equilibrium, there is already evidence of partial Wigner localization into patterns that are recognizable as predominantly (1,5) or (0,6).[8,31] Reimann *et al.*[31] had observed earlier that the ^1S ground state at $r_s = 4\,a_0^*$ had a predominantly (0,6) geometry, and Güçlü *et al.*[11] found that, as r_s increased further, this state transformed into a (1,5) geometry. From Fig. 6, we see that the transformation is quite complete by $r_s = 10\,a_0^*$.

We can analyze this phenomenon in more detail by considering the first excited ^1S state, which changes from predominantly (1,5) at $r_s = 4\,a_0^*$ to (0,6) at $r_s = 10\,a_0^*$. Thus, at $r_s = 4\,a_0^*$, the (1,5) and (0,6) isomers are inverted from their classical energy ordering, with the (1,5) isomer above the (0,6). By $r_s = 10\,a_0^*$, the classical ordering is reestablished, with (1,5) as the ground isomer, and the ordering stays this way for all higher r_s (see Ref. 17 and Fig. 4). At intermediate densities $r_s \approx 6\,a_0^*$, there is hybridization of the (1,5) and (0,6) isomers in both ^1S states.

As we noted in Sec. IV A, at $r_s \approx 6\,a_0^*$, the spin excitation energy (atomiclike exchange and correlation effects) is comparable to the nominal vibrational and isomeric excitation energies. There is no reason why the exchange and correlation effects in this case can not mix isomers for states with the same

values of L_z and S. We note that, as the spin excitation energy becomes significantly smaller than the isomeric excitation energy for $r_s \gtrsim 10\,a_0^*$ (see Fig. 3), the classical energy ordering of the (1,5) and (0,6) isomers is reestablished and the isomeric hybridization of the ground ^1S state disappears.

Note that the inversion of the (1,5) and (0,6) isomers only occurs for the $S = 0$ member of the ground-state spin multiplet. For the $S = 1$, 2, and 3 states (not shown), we find the (1,5) isomer to be below the (0,6) isomer already for $r_s \approx 2.75\,a_0^*$–$4\,a_0^*$ and for all higher r_s.

D. Generalization to larger sizes *N*

The main part of this paper is a case study for $N = 6$ electrons, but we can use the classical arguments that worked well for $N = 6$ (Sec. IV A) to show that aspects of the same excited-state phenomenology apply to larger N as well.

The classical model yields more than one isomer for $N = 6$ and for $N \geqslant 9$.[20,21] We have used the basin-hopping algorithm[29] to generate and study the classical isomers in the size range up to $N = 20$. As N increases, the energy separation of isomers tends to become smaller. Thus, the excitation energy $\Delta E_{\rm iso}(N)$ for N electrons satisfies $\Delta E_{\rm iso}(6) = 0.10\,\omega^{2/3}$, $\Delta E_{\rm iso}(9) = 0.044\,\omega^{2/3}$, and $\Delta E_{\rm iso}(19) = 0.013\,\omega^{2/3}$ (in effective a.u.). It is then generally the case that the first excited level (spin multiplet) for fixed L_z at intermediate r_s is an isomer rather than a vibrational excitation of the ground state. In fact, the crossovers between $\Delta E_{\rm iso}$ and $\Delta E_{\rm vib}$ (such that $\Delta E_{\rm vib}$ becomes smaller than $\Delta E_{\rm iso}$ for larger r_s) tend to occur for several hundred a_0^* or more for $N > 6$.[32] For example, for $N = 19$, the crossover occurs for $r_s \approx 800\,a_0^*$. We thus expect low-lying isomeric states to be a generic feature of the excitation spectrum of dots with $N = 6$ or $N \geqslant 9$ electrons at intermediate r_s values.

Also, the rotational excitation energies $\Delta E_{\rm rot}$ are generally found to be small compared to $\Delta E_{\rm iso}$ and $\Delta E_{\rm vib}$, similar to Fig. 3 for $N = 6$.

V. CONCLUSIONS

We have presented an accurate CI method, using a numerical basis set of mean-field type, that is capable of treating quasi-2D quantum dots (in the effective-mass approximation), with up to at least six confined electrons, at low electron densities $r_s \sim 50\,a_0^*$ in the strongly correlated regime of Wigner localization. Precise calculations of energies of low-lying states for $N = 6$ electrons at densities $r_s \approx 12\,a_0^*$–$16\,a_0^*$ achieve errors of order 1 part in 10^4 of the total energy (or better) and apparently reveal the fixed-node error in recent quantum Monte Carlo results (VMC–DMC).[9]

For six or more confined electrons, the excitation spectrum of Wigner molecule states at intermediate $r_s \gtrsim 3\,a_0^*$ involves isomeric excitations as well as rotational, vibrational, and spin excitations. By direct calculation with CI for $N = 6$ at $r_s = 50\,a_0^*$, we found that vibrational excitations had a qualitative correspondence with the classical normal modes for confined pointlike electrons, although the excitation energies only agreed approximately, and the energy ordering of the quantum vibrational modes could be different from the classical ones, presumably due to residual quantum fluctuations in the electron gas.

Since, at intermediate r_s, isomeric states are likely to be a low-lying excitation, it may be possible to observe them experimentally. As in molecules,[30,33] the selection rules for various processes such as optical absorption or inelastic scattering[12] can be strongly dependent on the isomers involved or the vibrational normal modes through the symmetry constraints. Theoretically, we found that a useful approach to interpreting the spectrum of CI eigenstates was to consider the pattern of allowed spins. It may be possible to make use of spin selection rules experimentally. Finally, recent improvements in high-spatial-resolution scanning probe techniques[34] may make it possible to observe the geometry of a Wigner molecule directly.

VI. ACKNOWLEDGMENTS

We gratefully acknowledge support from the European Commission through the EU-IndiaGrid2 network, *Sustainable e-Infrastructures across Europe and India*, Contract No. RI-246698.

APPENDIX: SYMMETRY-ALLOWED SPIN COUPLINGS

The consequences of the symmetry of localized Wigner states can be analyzed using the same group-theoretical methods that have been developed for planar (and nonplanar) molecules.[30,33] In this section, we outline instead a more elementary derivation that suffices in 2D to understand the sets of allowed spins in Table IV.

First, consider the stretched state $S_z = 3$ for total spin $S = 3$ and $L_z = 0$. The assignments of individual electron spins for the internal C_{5v} and C_{6v} molecular symmetries are represented pictorially in Figs. 7(a) and 7(b). Now, configuration 7(b) for C_{6v} is symmetric (+1) under a rotation through 1/6 of a turn ($\theta = \pi/3$). But this rotation is equivalent to a cyclic permutation of the six electrons (imagine enumerating the electrons 1 to 6 around the hexagon), which requires an *odd* number of electron interchanges and should yield a factor (−1) for fermionic antisymmetry. Therefore, $S = 3$ is incompatible with fermion antisymmetry and is excluded for C_{6v}.

In a similar way, configuration 7(a) for C_{5v} is also symmetric (+1) under a rotation through $\theta = 2\pi/5$, but this time there are an odd number of electrons in the outer ring, which yields an *even* number of fermion interchanges with the

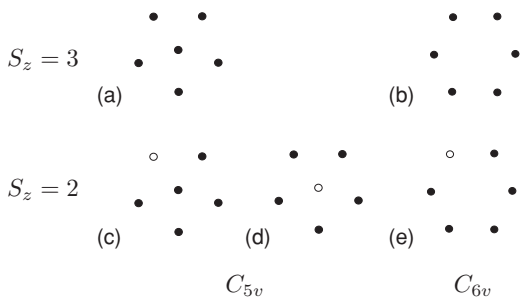

FIG. 7. Spin configurations for $S_z = 3$ (top row) and $S_z = 2$ (bottom row) for C_{5v} (left group) and C_{6v} (right group) molecular symmetries. A full circle indicates spin up, and an empty circle spin down.

required symmetry (+1). Therefore, $S = 3$ is compatible with fermion antisymmetry for C_{5v}.

We now proceed to $S_z = 2$ (still for $L_z = 0$). The distinct electron spin configurations for $S_z = 2$ are shown in Figs. 7(c)–7(e), where by distinct we mean that the configurations can not be transformed into each other under rotations. Now, configurations 7(c) and 7(e) with a spin-down electron in the outer ring have no symmetry under rotations, and there is thus no difficulty in constructing states from them with the required fermion antisymmetry. On the other hand, configuration 7(d) with a spin-down in the center is again symmetric under five-fold rotations, but as just discussed, this is compatible with fermion antisymmetry. We conclude that, for C_{6v} symmetry, there is one allowed $S = 2$ state. For C_{5v} symmetry, there are two allowed $S_z = 2$ configurations, but one of these corresponds to the $S = 3$ state found above, and so there is also one allowed $S = 2$ state for C_{5v}.

Continuing this procedure systematically for $S_z = 1$ and 0 yields straightforwardly the allowed spins $S = (0123)$ for C_{5v} and $S = (0012)$ for C_{6v} given in Table IV for $L_z = 0$.

The procedure for $L_z \neq 0$ is identical, except that now under a rotation through an angle θ we pick up an additional factor of $\exp(i\theta L_z)$, which can modify the conclusions. For instance, consider again the $S_z = 3$ configurations. A rotation of configuration (a) for C_{5v} through $\theta = 2\pi/5$ now yields a factor $\exp(i2\pi L_z/5)$. But, this can only equal +1 as required for fermions for $L_z = 0,5,10,\ldots$. Therefore, for $1 \leqslant L_z \leqslant 4$ (and cyclically with period 5 in L_z), the $S = 3$ state is forbidden for C_{5v}.

Similarly, a rotation of configuration 7(b) for C_{6v} through $\theta = \pi/3$ yields a phase $\exp(i\pi L_z/3)$, which can only equal -1 as required for fermions when $L_z = 3,9,15,\ldots$. Thus, $S = 3$ is forbidden for C_{6v} unless $L_z = 3$ (and cyclically with period 6 in L_z).

By continuing this procedure for $S_z = 2$, 1, and 0, one can readily deduce the spin patterns in columns (a) and (e) of Table IV.

So far, we have implicitly assumed the molecular state to be in the ground state of its vibrational modes, which is symmetric under rotations. When one vibrational quantum is present, the vibrational mode carries the symmetry of the corresponding normal-mode vector shown in Fig. 5. Now, the doubly degenerate modes in this figure can be arranged into linear combinations that contribute phases $\exp(\pm i|M|\theta)$ under rotations, with $|M| = 0$, 1, 2, or 3 according to the mode.[35] This is analogous to the effect of L_z, and so the allowed spins are simply those for $L_z^{\rm eff} = L_z \pm |M|$ for the C_{5v} isomer. As an example, consider a mode with dipolar symmetry $|M| = 1$ (such as the collective mode at $\Omega = \omega$ in Fig. 5) for $L_z = 1$. This gives $L_z^{\rm eff} = 0$ or 2, and so the allowed spins are $S = (0123)$ and $(01\bar{1}2)$ or (00111223). In this way, one sees that columns (b) and (d) in Table IV follow from an $|M| = 1$ dipolar normal mode, while column (c) can arise from a normal mode with either $|M| = 2$ (quadrupolar) or $|M| = 3$ (octupolar).

*steven.blundell@cea.fr
†sajeev.chacko@gmail.com; Present address: Centre for Computational Biology and Bioinformatics, Jawaharlal Nehru University, New Delhi 110 067, India.

[1] L. Jacak, P. Hawrylak, and A. Wójs, *Quantum Dots* (Springer, Berlin, 1998).
[2] R. Egger, W. Häusler, C. H. Mak, and H. Grabert, Phys. Rev. Lett. **82**, 3320 (1999); **83**, 462(E) (1999).
[3] C. Yannouleas and U. Landman, Phys. Rev. Lett. **82**, 5325 (1999).
[4] E. Wigner, Phys. Rev. **46**, 1002 (1934).
[5] V. M. Pudalov, M. D'Iorio, S. V. Kravchenko, and J. W. Campbell, Phys. Rev. Lett. **70**, 1866 (1993).
[6] A. Singha, V. Pellegrini, A. Pinczuk, L. N. Pfeiffer, K. W. West, and M. Rontani, Phys. Rev. Lett. **104**, 246802 (2010).
[7] M. Rontani, C. Cavazzoni, D. Bellucci, and G. Goldoni, J. Chem. Phys. **124**, 124102 (2006).
[8] A. Ghosal, A. D. Güçlü, C. J. Umrigar, D. Ullmo, and H. U. Baranger, Nat. Phys. **2**, 336 (2006).
[9] A. Ghosal, A. D. Güçlü, C. J. Umrigar, D. Ullmo, and H. U. Baranger, Phys. Rev. B **76**, 085341 (2007).
[10] C. Yannouleas and U. Landman, Rep. Prog. Phys. **70**, 2067 (2007).
[11] A. D. Güçlü, A. Ghosal, C. J. Umrigar, and H. U. Baranger, Phys. Rev. B **77**, 041301(R) (2008).
[12] S. Kalliakos, M. Rontani, V. Pellegrini, C. P. García, A. Pinczuk, G. Goldoni, E. Molinari, L. N. Pfeiffer, and K. W. West, Nat. Phys. **4**, 467 (2008).
[13] A. Szabo and N. Ostlund, *Modern Quantum Chemistry* (Dover, New York, 1996).
[14] C. Yannouleas and U. Landman, J. Phys. Condens. Matter **14**, L591 (2002).
[15] S. A. Blundell and K. Joshi, Phys. Rev. B **81**, 115323 (2010).
[16] F. Pederiva, C. J. Umrigar, and E. Lipparini, Phys. Rev. B **62**, 8120 (2000).
[17] S. A. Blundell and S. Chacko, Phys. Rev. B **81**, 121104(R) (2010).
[18] W. Häusler, Europhys. Lett. **49**, 231 (2000).
[19] C. Yannouleas and U. Landman, Phys. Rev. Lett. **85**, 1726 (2000).
[20] F. Bolton and U. Rössler, Superlattices Microstruct. **13**, 139 (1993).
[21] V. M. Bedanov and F. M. Peeters, Phys. Rev. B **49**, 2667 (1994).
[22] P. A. Maksym and T. Chakraborty, Phys. Rev. Lett. **65**, 108 (1990); Phys. Rev. B **45**, 1947 (1992).
[23] P. A. Maksym, Phys. Rev. B **53**, 10871 (1996).
[24] M. Manninen, S. Viefers, M. Koskinen, and S. M. Reimann, Phys. Rev. B **64**, 245322 (2001).
[25] G. Bastard, *Wave Mechanics Applied to Semiconductor Heterostructures* (Les Editions de Physique, Les Ulis, France, 1998).
[26] M. Koskinen, M. Manninen, and S. M. Reimann, Phys. Rev. Lett. **79**, 1389 (1997).
[27] K. Hirose and N. S. Wingreen, Phys. Rev. B **59**, 4604 (1999).
[28] R. G. Parr and W. Yang, *Density-Functional Theory of Atoms and Molecules* (Oxford University Press, New York, 1989).
[29] Z. Q. Li and H. A. Scheraga, Proc. Natl. Acad. Sci. USA **84**, 6611 (1987).

[30]G. Herzberg, *Molecular Spectra and Molecular Structure* (Van Nostrand, Princeton, 1967), Vol. 3.

[31]S. M. Reimann, M. Koskinen, and M. Manninen, Phys. Rev. B **62**, 8108 (2000).

[32]A possible exception occurs for certain low-frequency classical normal modes. Such modes exist where, in the pointlike classical model, there is a flat region of the potential-energy surface, typically associated with a slight distortion of one of the rings of electrons away from a perfectly regular circle (or ellipse). An example occurs for the excited isomer for $N = 6$ in Fig. 2(b), which is a staggered rather than regular hexagon. The low-frequency mode then corresponds to an oscillation back toward the perfectly regular structure. Another such mode occurs for the $N = 9$ ground-state isomer, and if there exists a corresponding quantum mode, the crossover between $\Delta E_{\rm iso}$ and $\Delta E_{\rm vib}$ would, in this case, occur at a smaller $r_s \approx 3a_0^*$. However, we note that according to the arguments of Sec. IV B, the flat classical potential-energy surface may not have a corresponding feature in the quantum case at intermediate r_s.

[33]J. M. Hollas, *Symmetry in Molecules* (Chapman and Hall, London, 1972).

[34]A. M. Mintairov, Y. Chu, Y. He, S. Blokhin, A. Nadtochy, M. Maximov, V. Tokranov, S. Oktyabrsky, and J. L. Merz, Phys. Rev. B **77**, 195322 (2008).

[35]Formally, the doubly degenerate normal-mode vectors in Fig. 5 transform under five-fold rotations as $\mathbf{u} \rightarrow \mathbf{u}' = \exp(\pm i|M|\theta_n)\mathbf{u}$, where $\theta_n = 2\pi n/5$ (with n an integer) is a symmetry rotation angle and $\mathbf{u}$ is an appropriate linear combination of the two degenerate normal-mode vectors shown in the figure. An analysis of the normal-mode vectors in Fig. 5 gives $|M| = 1$ (dipolar) for the modes at $\Omega = 0.650\omega$, $\Omega = \omega$, and $\Omega = 1.887\omega$; $|M| = 2$ (quadrupolar) for $\Omega = 1.223\omega$; $|M| = 3$ (octupolar) for $\Omega = 1.314\omega$; and $|M| = 0$ (scalar) for $\Omega = 1.732\omega$.